

RSC Advances



This is an *Accepted Manuscript*, which has been through the Royal Society of Chemistry peer review process and has been accepted for publication.

Accepted Manuscripts are published online shortly after acceptance, before technical editing, formatting and proof reading. Using this free service, authors can make their results available to the community, in citable form, before we publish the edited article. This *Accepted Manuscript* will be replaced by the edited, formatted and paginated article as soon as this is available.

You can find more information about *Accepted Manuscripts* in the [Information for Authors](#).

Please note that technical editing may introduce minor changes to the text and/or graphics, which may alter content. The journal's standard [Terms & Conditions](#) and the [Ethical guidelines](#) still apply. In no event shall the Royal Society of Chemistry be held responsible for any errors or omissions in this *Accepted Manuscript* or any consequences arising from the use of any information it contains.

Surfactant-modified Chemically Reduced Graphene Oxide for Electrochemical Supercapacitors

Qingqing Ke, Yanqiong Liu, Huajun Liu, Yu Zhang, Yating Hu, and John Wang*

Department of Materials Science and Engineering, National University of Singapore, Singapore 117574

*Email: msewangj@nus.edu.sg

Abstract: A facile method to synthesize surfactant-modified graphene for supercapacitor is demonstrated through intercalation of graphene oxide (GO) with Triblock copolymer Pluronic F127 (F127). A rationalized reduced GO-F127 is obtained by hydrothermal and thermal annealing-driven structural reconstruction. The F127 was found to be successfully intercalated in GO layers and facilitate the stabilization of the single layer or few-layers structure of graphene sheets during the reduction process. An increased surface area of 696 m²/g is achieved in the surfactant-modified graphene, which is about three times higher than that of pristine graphene (200 m²/g). The electrocapacitive behaviors of the resultant composites are systematically investigated by cyclic voltammeter and galvanostatic charge-discharge techniques. The sample of rGO-F127 thermal-treated at 400 °C delivers a maximum specific capacitance of 210 F/g at scanning rate of 1 mV/s in 6 M KOH electrolyte and an excellent cycling stability retaining over 95.6% of the initial capacity after 1000 cycles.

Keywords: Surfactant, graphene, supercapacitors, Pluronic F127.

1. Introduction

Graphene is a light-weight two-dimensional monolayer composed of all-sp²-hybridized carbons with intriguing properties, such as high electrical conductivity, high surface area, good mechanical properties, which make it highly attractive for numerous applications including Li-ion batteries, fuel cells, chemical detectors, solar cells and supercapacitors.¹⁻⁵ As an intriguing approach for production of graphene, reduction of graphene oxide (GO) by thermal method or reducing agent has attracted intensive studies.⁶⁻⁹ Fortunately, GO can be facily derived from oxidation of natural graphite in a large scale, allowing the GO to be an exciting precursor for producing graphene based materials with low cost.¹⁰ An atomic layer of GO generally comprises with phenol hydroxyl and epoxide groups on the basal plane and ionizable carboxylic acid groups around the edges.^{11,12} Normally, through weak dipole and quadrupole van der Waal's interaction with surrounding environment, the ionized edge acid groups enable the stabilization of GO in aqueous dispersion in the form of single sheet layer. However, removing the oxygen-containing groups by chemical reduction, often introduces a quick re-aggregation of graphene sheets into graphite. Therefore, the microstructures of the resultant rGO should be modulated by a proper assembly strategy, which significantly affects the properties in the final product.

GO has been reported to be an unique amphiphile with negative charged hydrophilic edges and hydrophobic basal plane.^{13,14} This intriguing behavior allows GO to be selectively interacted with certain surfactants, which are capable of tuning the amphiphilicity of GO and controlling the assembling of the rGO at interface. For example, Zhang *et al.* have investigated the surfactant-stabilized graphene materials with different surfactants of tetrabutylammonium hydroxide (TBAOH), cetyltrimethylammonium bromide (CTAB), and sodium dodecylbenzene sulfonate

(SDBS).¹³ They showed that the rGO sheets could be intercalated by the surfactants, which eliminate the restacking of rGO and increase its wettability, thus leading to an improved electrochemical performance. In addition, the modification by surfactant helps to homogeneously disperse rGO into single or few layers in aqueous solutions, which permits chemical reactions between rGO and second phase in aqueous solvent. Mao *et al.* have directly loaded the PANI onto surfactant-stabilized rGO in aqueous solvent, which avoids the general degradation of PANI during the reduction and re-oxidation process of GO.¹⁵ Among the large family of surfactants, the commercially available block copolymer PEO₁₀₆-PPO₇₀-PEO₁₀₆ (F127) has been widely investigated due to its well established chemical behaviors.¹⁶ It shows that such block copolymer can be self-assembled through hydrogen bonding and hydrophobic/hydrophilic interactions in aqueous environments to form vesicles, which can be used as soft templates for fabricating mesoporous carbon materials.¹⁷⁻¹⁹ However, few works have been conducted to control the assembling of graphene by F127 in the electrochemical field. In the present work, we modulated the microstructure of graphene by intercalating the surfactant of F127 into the layered GO, which is further processed by hydrothermal and thermal annealing procedures. The electrocapacitive behavior of the surfactant-modified rGO is systematically investigated by cyclic voltammeter and galvanostatic charge-discharge techniques. The improved electrochemical performance is demonstrated for the surfactant-modified rGO, contributed from the increased surface area and more favorable pore volumes, as compared to the pristine rGO.

2. Experimental

2.1 Materials

Pluronic F127 (M_{av} =12000 g/mol) was purchased from Sigma-Aldrich. GO solution (5 g/l) was obtained from Graphite Mar

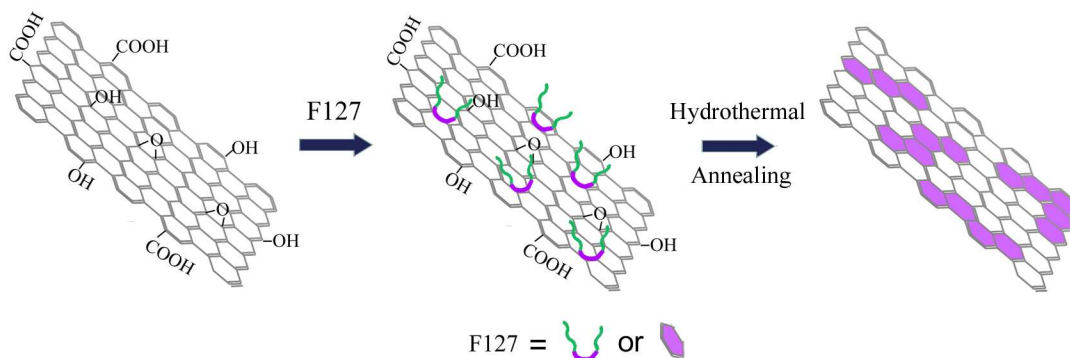


Fig. 1 Schematic illustration for the synthesis of rGO-F127 composites *via* hydrothermal and thermal annealing routes. Note that the structure of F127 is divided into the PPO and PEO parts represented by lines in purple and green colors respectively. After drying, the long-tailed F127 is cross-linked, as indicated by the purple hexagon.

ket. All the chemical reagents used in this work were commercially available and used as received without any purification.

2.2 Preparation of surfactant-stabilized graphene (rGO-F127)

In a typical experiment, 12.5 mg F127 was added into 20 mL dilute water and stirred at room temperature for 24 hrs. The well dissolved solution is then added into 5 mL GO aqueous solution at a concentration of 5 g/L. The mixture is then stirred for another 24 hrs to make sure that the surfactant is well intercalated between the GO sheet layers. After that, the suspension solution was transferred to a Teflon-lined autoclave and heated to 180 °C for 12 hours. The autoclave was then cooled to room temperature. There was precipitation at the bottom of the autoclave as black powder for the hydrothermally treated rGO-F127 composites. The black powder was recovered and freeze-dried by liquid nitrogen, and then freeze dried under vacuum condition. The as-synthesized rGO-F127 composites were then annealed in argon at different temperatures of 350 °C, 400 °C and 450 °C respectively (labeled as rGO-F127-350, rGO-F127-400, rGO-F127-450 respectively.) The composite without any heat treatment (labeled as rGO-F127-non) was prepared at the same condition. For comparison purpose, samples of pure rGO were annealed at different temperature of 350 °C, 400 °C and 450 °C (labeled as rGO-350, rGO-400, rGO-450 respectively).

2.3 Characterization.

The rGO-F127 composites were characterized using both scanning electron microscopy (SEM, JOEL JSM-6700F) and transmission electron microscopy (TEM, JOEL JEM-2010). N₂ sorption isotherms were measured for specific surface area and pore size distribution (ASAP 2020). Before measurement, each sample was degassed at 180 °C for 1 hour. The specific surface area and pore volume were measured by N₂ adsorption/desorption using Brunauer-Emmet-Tell (BET, Micromeritics ASAP2020) method. The composition and structure were studied by a Kratos Axis Ultra X-ray photoelectron spectroscopy (Kratos Analytical) equipped with a monochromatized Al K α X-ray source, where the pressure of the chamber was controlled at 10⁻⁹ torr. Thermogravimetric Analysis (TGA) utilized the SDTQ600 instrument. The chamber was purged with N₂ gas (7.5 ml/min) and heated from room temperature to 650 °C with heating rate of 10 °C/min. Fourier transform infrared (FT-IR) spectra were examined on a Varian 3100 FT-IR (Excalibur series) spectrophotometer. Samples were

prepared by casting pellets from sample/KBr mixtures. Sixty-four scans were signal averaged with a resolution of 4 cm⁻¹ at room temperature.

2.4 Electrochemical Measurement

Cyclic voltammetry (CV) and galvanostatic charge-discharge were characterized for the electrode using 6 M KOH as electrolyte in a three-electrode cell using Solartron Electrochemical System SI 1287. A platinum plate is used as the counter electrode and Ag/AgCl (in a saturated KCl aqueous solution) as the reference electrode. 80 wt% of surfactant-modified rGO, 10 wt% of acetylene black, and 10 wt% of polytetrafluoroethylene (PTFE) were mixed together in ethanol, and then ultrasonicated to ensure uniform mixing. The mixed slurry was coated onto a Ni foam, then dried at 120 °C in vacuum oven for 12 hours. The loading mass of samples was kept around 7 mg. The electrodes were pressed at 8 MPa, then kept at 120 °C in air to remove extra water.

3. Results and discussion

The formation procedure of F127-rGO composites took place in the following three steps: GO was first soaked with F127. GO is an amphiphile with hydrophilic edges and hydrophobic basal plane (as shown in Fig. 1).²⁰ Therefore, the hydrophobic part of PPO in F127 can in principle interact with the hydrophobic part of GO, while the hydrophilic segment of PEO will interact with the surrounding water molecules through forming hydrogen bonds.²¹ In the next process, the oxygen-containing group in the GO is removed by hydrothermal treatment at 180 °C for 12 hrs. Due to the modification by adding F127, the hydrophilic PEO chains in the rGO-F127 composites stabilize the graphene layer in the water and suppress the restacking of graphene sheets during the hydrothermal process.²¹ After thermal treatment, the long-tailed F127 in the as-designed system is supposed to be cross-linked into nanoflakes to decorate graphene layers, acting as spacers to eliminate the agglomeration of graphene into graphite. However, we also note that the presence of F127 will decrease the overall conductivity due to the high resistance as compared to graphene. Therefore, in the last procedure of sample preparation, the content of F127 is rationalized through different thermal treatment in order to improve the electrochemical performance of hybrid electrode.²²

The composition of the surfactant stabilized rGO is firstly studied by TGA as shown in Fig. 2. Three distinctly weight loss

steps are observed in Fig. 2. At temperatures below 100 °C, the weight loss around 6% is attributed to the water vapor. The major weight loss is about 21% occurring at temperatures between 200 to 300 °C, which is related to the removal of oxygen-containing groups from rGO.^{23,24} When the temperature is raised above 350 °C, the decomposition of the F127 occurs and a weight loss of 6% is obtained.²⁵

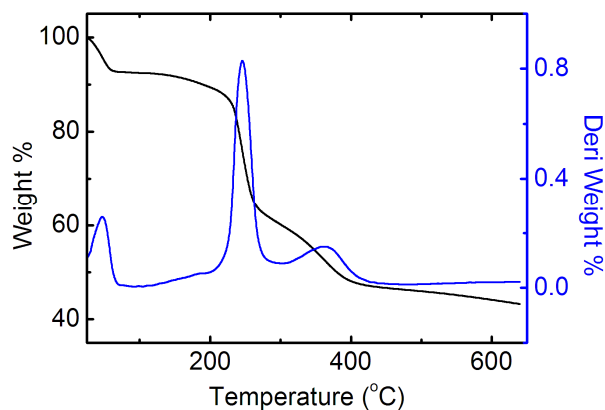


Fig. 2 TGA curves of as-derived F127-rGO composite.

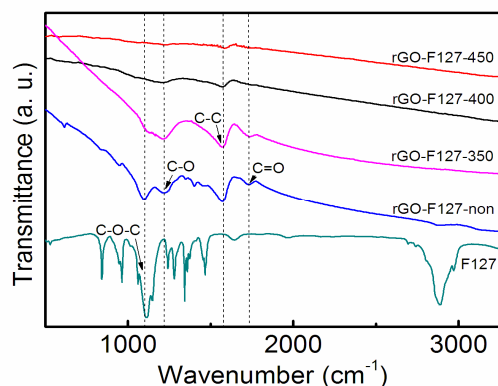


Fig. 3 FT-IR spectra of F127, rGO-F127-non, rGO-F127-350, rGO-F127-400 and rGO-F127-450.

Fig. 3 presents the FT-IR spectra of F127 and rGO-F127 hybrids with different thermal treatments. As shown in these spectra, the band locating around 1100 cm^{-1} is assigned to the characteristic C-O-C stretching vibration in F127, which are found to gradually disappear in samples thermal-treated with increasing temperatures.²⁶ It evidences that the content of F127 is reduced with increasing annealing temperatures. This result is consistent with observation from TGA. The FTIR peaks at 1731 cm^{-1} and 1222 cm^{-1} are attributed to carbonyl/carboxyl (C=O) and epoxy (C-O) respectively, while the peak appearing at 1571 cm^{-1} is corresponding to the deformed C-C bond due to the existence of epoxy groups.²⁷ The peaks of C=O and C-O become weaker with increasing annealing temperature, as indicative of removal of the oxygen-containing groups during thermal treatment process.

The morphology of rGO-F127 composites annealed at different temperatures was characterized by SEM as shown in Fig. 4. All F127-rGO composites exhibit 3D porous structures, formed during the hydrothermal process.²⁸ In addition to the porous structure, one also notes that certain bulk-like F127 is covered on the rGO sheets in rGO-F127-non and rGO-

F127-350. With further increasing annealing temperature, the gauzy graphene sheets are formed and exhibit a curved thin flaky appearance as shown in the corresponding SEM images. The detailed nanostructure of the surfactant modified rGO is investigated by the high resolution TEM images. For the surfactant-stabilized graphene materials (as shown in inset of Fig. 5), the gauze graphene with the disordered or irregular stacked layers is observed, demonstrating that the graphene sheets are in the single or few layers structures.¹³ With increasing the annealing temperature, the nanostructure and morphology of a single sheet are varied. For the as-obtained rGO-F127 composite, the sphere-like cross-linked F127 are uniformly decorated on the graphene sheets. Upon thermal treatment, bright regions in irregular piece-like shape are observed as indicated by the black arrows in Fig. 5 b and c, evidencing that the uniformly covered F127 is partially removed from the graphene layer. When the annealing temperature is raised to 450 °C, the F127 is completely removed and graphene sheets with a dense of the microspheres are exposed.²⁸

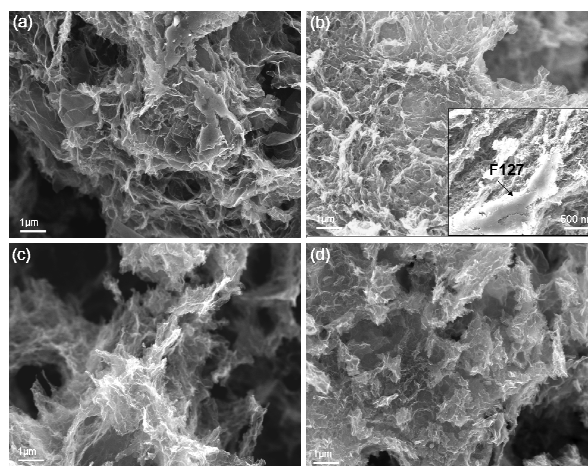


Fig. 4 SEM images for composites of rGO-F127 without annealing treatment (a) and annealed at temperatures of 350 °C (b), 400 °C (c) and 450 °C (d), respectively.

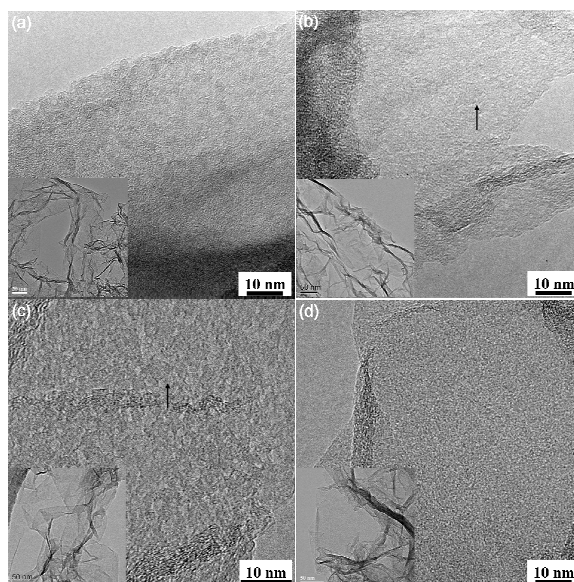


Fig. 5 TEM images showing the individual sheet layer of rGO-F127-non (a), rGO-F127-350 (b), rGO-F127-400 (c) and rGO-F127-450 (d).

rGO-F127-450 (d). The insets are the low resolution image of the

corresponding samples.

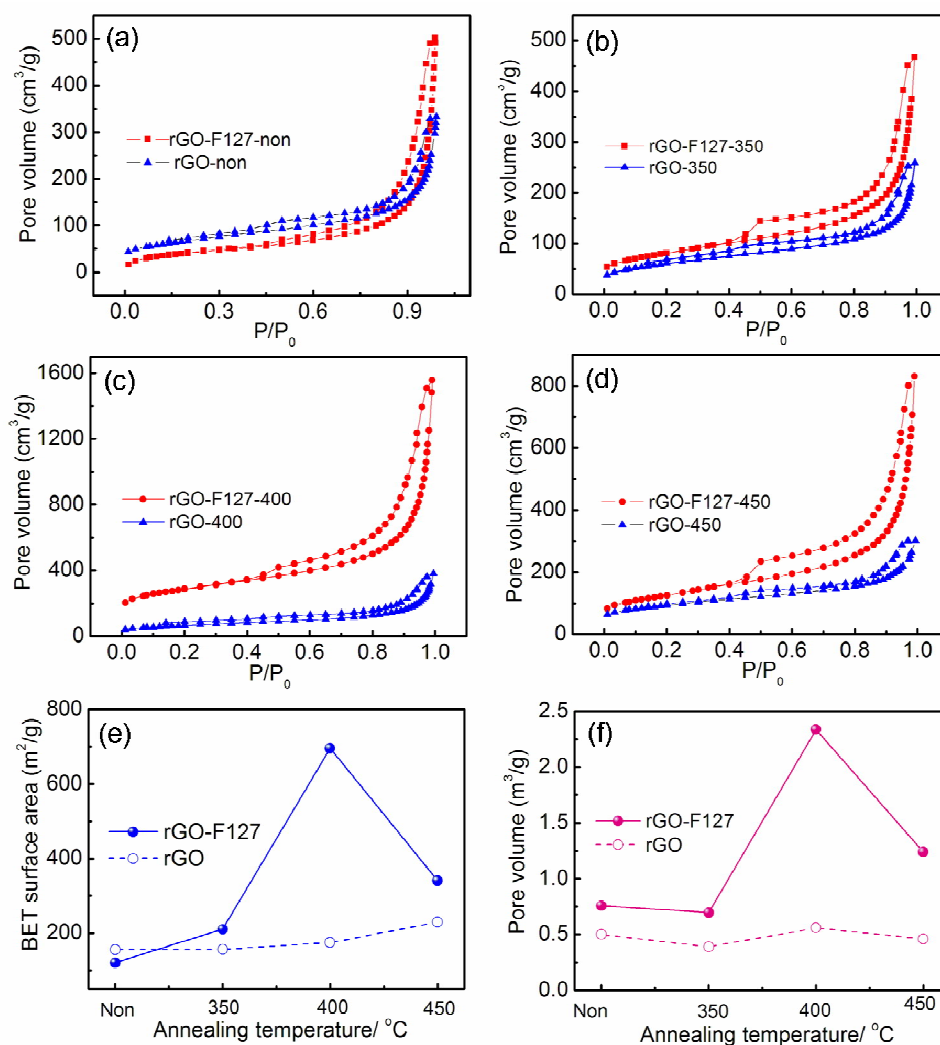


Fig. 6 The N₂ adsorption-desorption isotherms for rGO-F127 and rGO without heat treatment (a) and those annealed at 350 °C (b), 400 °C (c) and 450 °C (d). The BET surface and pore volume for the rGO-F127 and rGO with different annealing temperatures are shown in (e) and (f) respectively.

The specific surface areas for rGO-F127 composites and rGO with different heat treatments were examined by using isothermal N₂ adsorption-desorption as shown in Fig. 6. They all show the cross-curves between type-I and type-IV curves, demonstrating the presence of micro/mesopores in these materials. Compared to the isothermal curves between the rGO (in blue lines) and rGO-F127 (in red lines), the amount of gas absorption is greatly enhanced in rGO-F127 composites, indicating a rise in specific surface areas of these surfactant modified rGO materials. The calculation of BET surface areas for the rGO-F127 (in solid lines) and rGO (in dashed lines) with different heat treatment are plotted in Fig. 6e. It shows that the BET surface areas of rGO-F127 composites are largely dependent on the heat treatment, while those of rGO show a small variation (keep around 200 m²/g) with the annealing temperatures ranging from room temperature to 450 °C. The BET surface areas of rGO-F127 composites are greatly enhanced compared those of rGO at the same annealing temperatures. In particular, rGO-F127-400 shows an advantageous value of 696 m²/g, which is almost three times higher than that of the

pristine rGO. This result clearly shows that a great enhancement in surface area originates from the modification of F127 rather than the heat treatment. Moreover, a similar trend is also observed for the variation of pore volume as a function of annealing temperatures (shown in Fig. 6f). The corresponding pore volumes of rGO are independent of the heat treatment process, while a great improvement in pore volume is found in the surfactant modified rGO composites. Notably, rGO-F127-400 also performs a favorable pore volume of 2.34 cm³/g. The enlarged pore volume observed in the rGO-F127 composites is believed to be beneficial for the diffusion of the electrolyte to the active sites of electrode and will make a positive contribution to the electrochemical performance.²²

Defects and oxygen-containing functionalities on rGO surface degrade the overall conductivity, therefore leading to a poor electrochemical performance. Herein, the recovery of benzene ring for rGO and rGO-F127 composites at different annealing temperatures is examined by XPS survey and shown in Fig. 7. The XPS

spectrum of C 1s collected from the six samples can be deconvoluted into three peaks (colored lines) with different carbon bonds:

sp^2 bonded carbon at 284.5 eV (C-C), epoxy/hydroxyls at 286.4

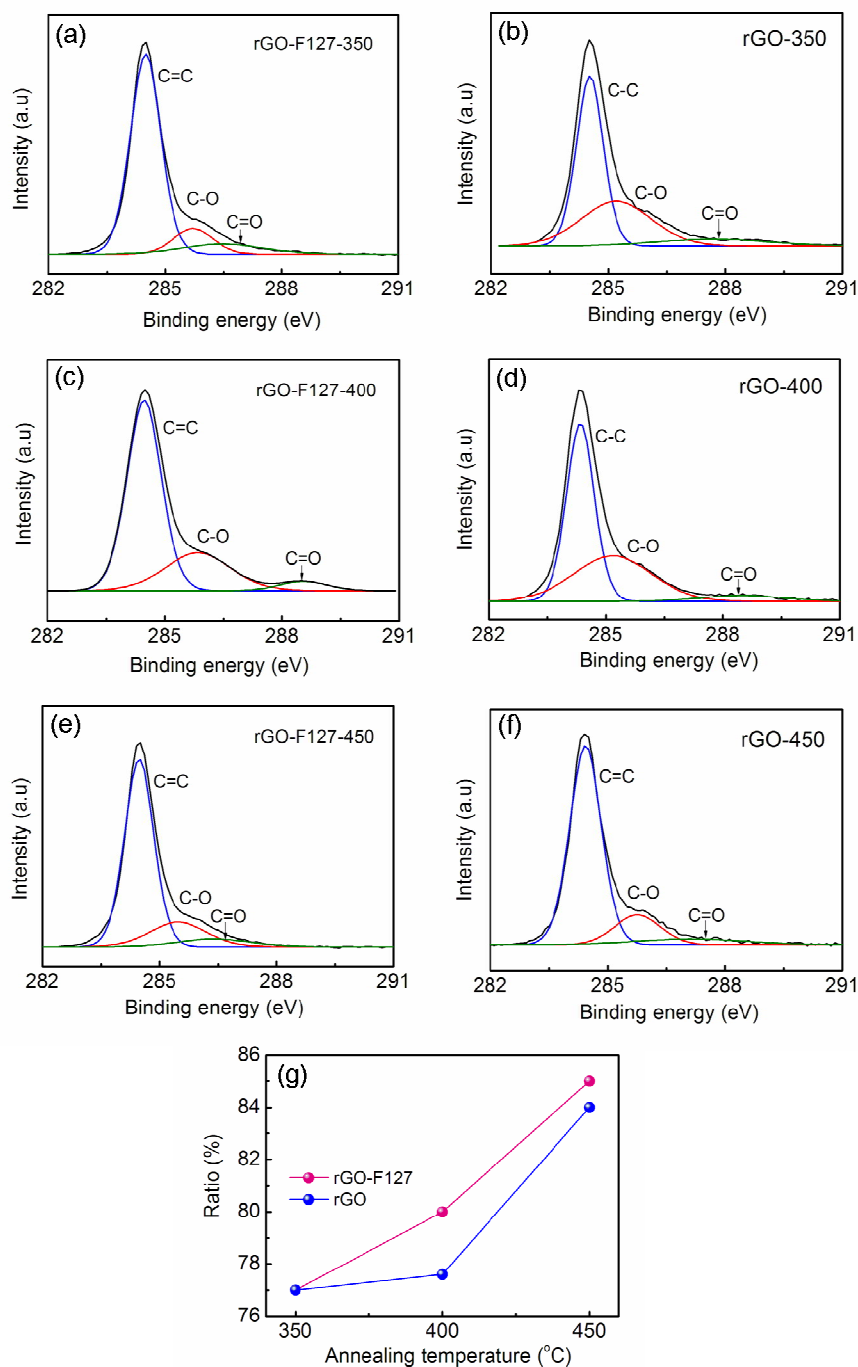


Fig. 7 C 1s XPS spectra of rGO-F127 annealed at temperatures of 350 °C (a), 400 °C (c) and 450 °C (d), respectively. The C 1s XPS spectra of rGO annealed at the same condition is shown in (b), (d) and (f) respectively. The comparison of the C-C contents between rGO (in blue color) and rGO-F127 composites (in red color) are plotted in (g).

eV (C-O), and carbonyls at 288.4 eV (C=O). The resultant carbon ratios can be calculated from the fitted peak areas and the estimated carbon ratios are summarized in Fig. 7g. It shows that the C-C ratio in rGO and rGO-F127 composites exhibits the similar value of 77% at temperature of 350 °C, while both of rGO and rGO-F127 samples show a rise in the recovery of benzene ring with increase in the annealing temperature. This result is consistent with previous reports that the thermal-annealing method is capa-

ble of facilitating the removal of the oxygen-containing groups.²⁴ Additionally, we also note that the degree of carbon recovery is higher in surfactant modified rGO than that of rGO. For example, the C-C ratio of rGO-F127-400 is greatly enhanced from 77% to 80% as compared to that of rGO-400. With further increasing the annealing temperature to 450 °C, oxygen-containing groups are largely removed from rGO surface and the reduction degree is around 85% achieved for the rGO-F127-450.

To evaluate the electrochemical behavior of the rGO-F127 composites, cyclic voltammetry (CV) and galvanostatic charge-

discharge were conducted in 6 mol/L KOH electrolyte. Fig. 8a

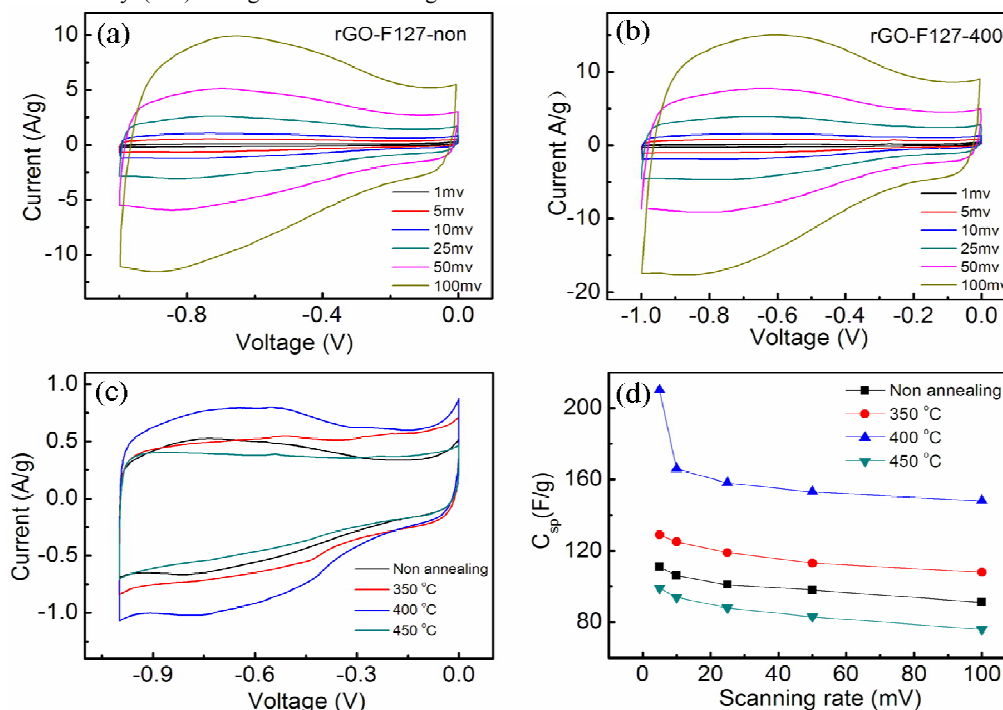


Fig. 8 Steady state cyclic voltammograms of rGO-F127-non (a), and rGO-F127-400 (b) supercapacitors, measured by applying a potential varying from -1 to 0 V at varying sweep rates (from 1 to 100 mV/s). Comparison of CV curves for rGO-F127 composites with different heat treatments at the scan rate of 1 mV/s (c). Specific capacitance of the four samples with respect to different scan rates (d).

and b show the CV curves of the rGO-F127-non and rGO-F127-400 at various sweep rates. Both electrodes demonstrate a rise in current response with increasing sweep rate, indicating a desirable capacitive behavior. Besides, the two samples present CV curves with the occurrence of not only rectangular-like shape, but also a few humps, which is owing to the presence of pseudocapacitance. Fig. 8c shows the CV curves for the different heat-treated rGO-F127 composites at the scan rate of 1 mV/s measured in three-electrode configuration. The CV curves for the four samples present almost rectangular shape, as indicative of dominant capacitive contribution from EDLC. Few humps located at the voltage ranging from -0.8 V to -0.4 V are observed in CV curves of the samples annealed below 400 °C, while those of rGO-F127-450 show a nearly ideal rectangular shape. Normally, the humps in the CV curves originate from the contribution from the oxygen-containing group.²⁵ In the XPS survey, we also note that the thermal annealing can effectively remove the oxygen-containing groups from the rGO surface. Therefore, with increasing annealing temperature, the largely lost oxygen-containing groups is responsible for the nearly absence of the humps in CV curves in rGO-F127-450. The specific capacitance obtained from the CV curves can be estimated by the following equation:

$$C = \frac{\int IdV}{2\mu m\Delta V} \quad (1)$$

where I is the response current, V is the potential scan rate, ΔV is the potential window, m is the mass of active electrode material and μ (mV s^{-1}) is the scan rate. The specific capacitances calculated for the four samples are summarized in Fig. 8d, which are plotted as a function of potential scan rate. The capacitance values are of 111, 129, 210 and 99 F/g for rGO-F127-non, rGO-F127-

350, rGO-F127-400 and rGO-F127-450, respectively at the scan rate of 1 mV/s. As expected, the capacitances of these samples decrease with increasing the scan rate, which is related to intercalation/deintercalation of protons or alkaline metal cations. At low scan rates (e.g., 1 mV/s), protons or alkaline metal cations can intercalate into the inner of the electrode material, which can be fully utilized. In contrast, a higher scan rate only permits protons or alkaline metal cations intercalate/deintercalate into the out layer of the electrode, therefore giving rise to the modest electrochemical performance.²⁹ Compared with the other three samples, the rGO-F127-400 shows an increased surface area and more favorable pore volumes, which allow ions transfer into electrodes more efficiently and therefore give rise to a better performance especially at low scan rates.

At temperatures below 400 °C, the capacitive performance is increased with the rise in annealing temperature. Especially, at the temperature of 400 °C, an advantageous capacitance of 210 F/g is achieved, which is almost two times higher than that of rGO-F127-non (111 F/g) and rGO-F127-350 (129 F/g). When the annealing temperature is raised to 450 °C, an evidently decrease in specific capacitance is however observed in rGO-F127-450 (99 F/g). Notably, the trend of change in capacitance during the heat treatment process largely follows that of the variation in BET surface area and pore volume with the annealing temperature. The rise in specific capacitance at temperatures below 400 °C is owing to the enlarged surface area and pore volume, which can effectively facilitate the diffusion of the electrolyte ions into the electrode. In addition, we note that the lowest capacitance is found in the rGO-F127-450, which possessing a higher surface area and pore volume than that of rGO-F127-non or rGO-F127-350. It manifests that the electrochemical performance of rGO-F127 composites is

not solely determined by the surface area or the pore volume.²⁵ The presence of surfactants in graphene materials is believed to

enhance the wettability of the graphene surface and thus capable

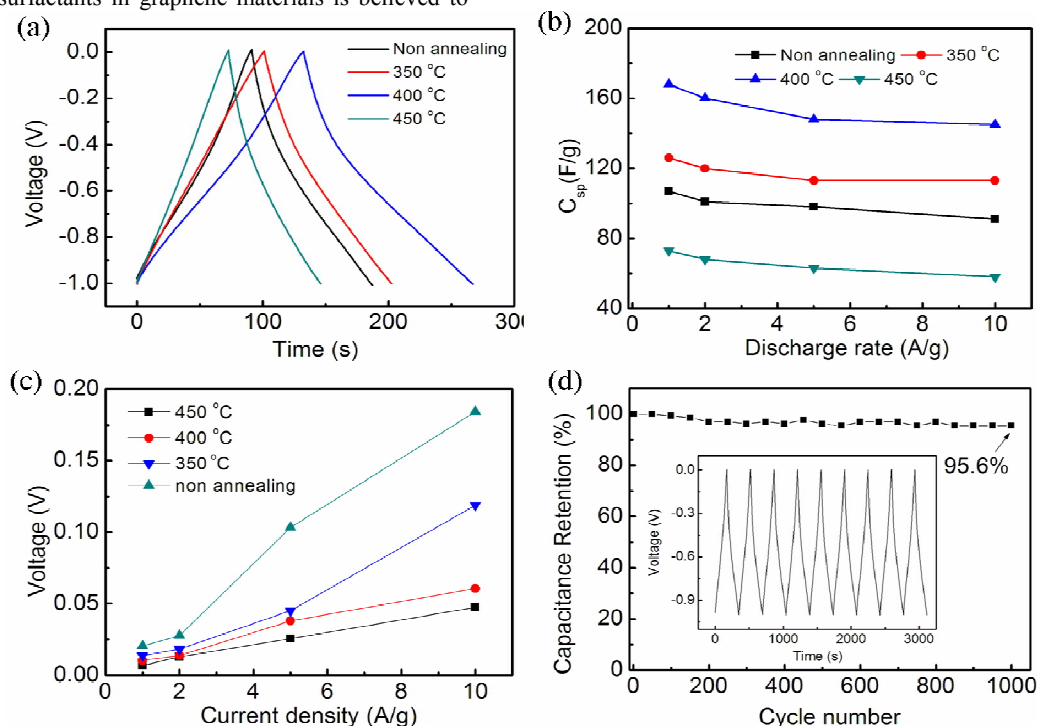


Fig. 9 (a) Galvanostatic charge-discharge curves for rGO-F127 composites at the current density of 1 A/g, (b) variation of specific capacitance at different current densities, (c) variation of IR drop with discharge current density, and (d) cycling performance at the current density of 1 A/g.

Table 1 Physicochemical parameters of rGO-F127-non, rGO-F127-350, rGO-F127-400, rGO-F127-450.

Sample	BET surface area	Pore volume	C=C ratio	ERS /ohm	Csp F/g
rGO-F127-non	121	0.75799	-	1.8e-2	107
rGO-F127-350	211	0.69703	77%	1.2e-2	126
rGO-F127-400	696	2.33518	80%	5.7e-3	168
rGO-F127-450	341	1.23857	85%	4.5e-3	73

of boosting the electrochemical performance as a supercapacitor electrode.¹⁵ When the annealing temperature is raised up to 450 °C, the surfactant of F127 is largely decomposed, leading to a weak wettability of rGO layers in rGO-F127-450. It makes the diffusion of electrolyte ions within the sample difficult and therefore contributes to a bad electrochemical performance.

The capacitive performance is further studied by galvanostatic charge-discharge scanning with different current densities in the voltage window ranging from -1 to 0 V. Fig. 9a shows the galvanostatic charge-discharge for the rGO-F127 composites at the current density of 1 A/g. The charge/discharge plots for these five samples show a triangular shape and nearly symmetric profile, suggesting the dominant contribution from EDLC, while a slight asymmetry is resulted from the pseudocapacitive behavior of oxygen-containing groups. In the charge-discharge profile, rGO-

F127-400 shows the largest discharge time, whereas rGO-F127-350, rGO-F127-non electrodes show a slightly reduced discharge time, and the rGO-F127-450 offers the shortest discharge time. This observation suggests that rGO-F127-400 exhibits the highest capacitance value (168 F/g), followed by rGO-F127-350 (126 F/g), rGO-F127-non (107 F/g) and rGO-F127-450 (73 F/g), which is consistent with trend obtained from the CV testing. In addition, we also note that the specific capacitance achieved for rGO-F127-400 (168 F/g) is much more advantageous than that of rGO (101 F/g) alone at the same measurement condition. This improvement is owing to the enhanced surface area and pore volume induced by the modification of F127, which are more favorable for ion diffusion, as discussed earlier. To evaluate the capacitance retention of surfactant modified rGO electrode materials at high current density, Fig. 9b shows the variation of specific capacitance at different

current densities. It shows that a nearly stable capacitance value at high current densities, suggesting a desirable retention capability. Fig. 9c shows that the IR drop increases almost linearly against the discharge current density for the rGO-F127 composite electrodes and the overall equivalent series resistance (ESR) of the supercapacitor cell can be determined from the slope of the linear relationship. Internal resistances increase with increasing annealing temperature. The calculated ESR values are summarized in Table 1, showing that rGO-F127-non, rGO-F127-350, rGO-F127-400, and rGO-F127-450 are of 1.8×10^{-2} ohm, 1.2×10^{-2} ohm, 5.7×10^{-3} ohm and 4.5×10^{-3} ohm, respectively. The improved conductivity with increasing the annealing temperature can be correlated to the increased reduction of carbon in rGO and removal of F127, which is of high resistance. The decrease in internal resistance is highly desirable for energy storage, as less energy will be lost to produce the unwanted heat during charging/discharging cycles. The cycle life of rGO-F127-400 was further examined by using the continuous charge-discharge experiment at a current density of 1 A/g. The capacitance retention is shown in Fig. 9d, as a function of cycle number (cycled between -1 and 0 V). A typical triangular charge-discharge curve is observed as shown in the inset of Fig. 9d, indicating that the EDLC energy storage is dominant. A slight decrease in capacitance over the first 200 cycles and remains almost unchanged thereafter. The degradation in capacitance can well be ascribed to the consumption of electrolyte arising from the irreversible reaction between the electrodes and electrolyte.³⁰ The cycling performance of the rGO-F127-400 retains 95.6 % of its initial capacity over 1000 cycles, revealing an excellent stability for supercapacitor application.

4. Conclusions

Surfactant-modified graphene materials were developed for supercapacitor by intercalation of graphene oxide (GO) with Triblock copolymer Pluronic F127, followed by hydrothermal treatment and thermal annealing to rationalize the nanostructures. F127 was successfully intercalated between the rGO sheet layers, leading to an increased surface area and pore volume as well as an enhanced surface wettability, which contribute to the improved electrochemical performance. A specific capacitance of 210 F/g is measured for the rGO-F127-400 at scanning rate of 1 mV/s in 6 M KOH electrolyte. This material also shows an excellent cycling stability of 95.6 % after 1000 cycles of consecutive galvanostatic charge-discharge, demonstrating a desirable performance for electrochemical energy storage.

Acknowledgements

We are grateful for the financial support from the Agency for Science, Technology and Research of A-Star in Singapore (Grant number: 1121202013).

References

- Z. S. Wu, W. Ren, L. Wen, L. Gao, J. Zhao, Z. Chen, G. Zhou, F. Li, H. M. Cheng, *ACS Nano*, 2010, **4**, 3187-3194.
- F. Schedin, A. K. Geim, S. V. Morozov, E. W. Hill, P. Blake, M. I. Katsnelson, K. S. Novoselov, *Nat. Mater.*, 2007, **6**, 652-655.
- L. Valentini, M. Cardinali, S. B. Bon, D. Bagnis, R. Verdejo, M. A. Lopez-Manchado, J. M. Kenny, *J. Mater. Chem.* 2010, **20**, 995-1000.
- L. L. Zhang, R. Zhou, X. S. Zhao, *J. Mater. Chem.* 2010, **20**, 5983-5992.
- Y. Cai, A. Zhang, Y. P. Feng, C. Zhang, H. F. Teoh, and G. W. Ho, *J. Chem. Phys.*, 2009, **131**, 224701.
- W. Gao, L. B. Alemany, L. Ci and P. M. Ajayan, *Nat. Chem.*, 2009, **1**, 403-408.
- S. Park and R. S. Ruoff, *Nat. Nanotechnol.*, 2009, **4**, 217-224.
- W. Zhou, J. Zhu, C. Cheng, J. Liu, H. Yang, C. Cong, C. Guan, X. Jia, H. J. Fan, Q. Yan, C. M. Li, T. Yu, *Energy Environ. Sci.*, 2011, **4**, 4954-4961.
- X. Chen, X. Chen, F. Zhang, Z. Yang, S. Huang, *J. Power Sources*, 2013, **243**, 555-561.
- K. Zhang, L. L. Zhang, X. S. Zhao and J. Wu, *Chem. Mater.*, 2010, **22**, 1392-1401.
- W. Cai, R. D. Piner, F. J. Stadermann, S. Park, M. A. Shaibat, Y. Ishii, D. Yang, A. Velamakanni, S. J. An, M. Stoller, J. An, D. Chen and R. S. Ruoff, *Science*, 2008, **321**, 1815-1817.
- Y. Cai, A. Zhang, Y. P. Feng, and C. Zhang, *J. Chem. Phys.*, 2011, **135**, 184703
- K. Zhang, L. Mao, L. L. Zhang, H. S. O. Chan, X. S. Zhao and J. Wu, *J. Mater. Chem.*, 2011, **21**, 7302-7307.
- H. R. Byon, S. W. Lee, S. Chen, P. T. Hammond, Y. Shao-Horn, *Carbon*, 2011, **49**, 457-467.
- L. Mao, K. Zhang, H. S. O. Chan and J. Wu, *J. Mater. Chem.*, 2012, **22**, 80-85.
- C. Liang, Z. Li, S. Dai, *Angew. Chem., Int. Ed.* 2008, **47**, 3696-3717.
- L. Lai, G. Huang, X. Wang, J. Weng, *Carbon* 2010, **48**, 3145-3156.
- Z-C Yang, Y. Zhang, J-H Kong, S. Y. Wong, X. Li, J. Wang, *Chem. Mater.* 2013, **25**, 704-710.
- Z-C Yang, C-H Tang, H. Gong, X. Li, J. Wang, *Journal of Power Sources*, 2013, **240**, 713-720
- J. Kim, L. J. Cote, F. Kim, W. Yuan, K. R. Shull and J. Huang, *J. Am. Chem. Soc.*, 2010, **132**, 8180-8186.
- S. Li, J. Guo, R. A. Patel, A. L. Dadlani, R. M. Leblanc, *Langmuir*, 2013, **29**, 5742-5748.
- H. Liu, Y. Zhang, Q. Ke, K. H. Ho, Y. Hu and J. Wang, *J. Mater. Chem. A*, 2013, **1**, 12683-12694.
- S. Some, Y. Kim, Y. Yoon, H. Yoo, S. Lee, Y. Park and H. Lee, *Sci. Rep.*, 2013, **3**, 1929.
- L. L. Zhang, X. Zhao, M. D. Stoller, Y. Zhu, H. Ji, S. Murali, Y. Wu, S. Peralas, B. Clevenger, R. S. Ruoff, *Nano Lett.*, 2012, **12**, 1806-1812.
- M. Li, J. Ding, J. Xue, *J. Mater. Chem. A*, 2013, **1**, 7469-7476.
- Q. Zhou, Z. Zhang, T. Chen, X. Guo, S. Zhou, *Colloids Surf., B*, 2011, **86**, 45-57.
- A. Bagri, C. Mattevi, M. Acik, Y. J. Chabal, M. Chhowalla and V. B. Shenoy, *Nat. Chem.*, 2010, **2**, 581-587.
- Z. Li, J. Wang, S. Liua, X. Liu, S. Yang, *J. Power Sources*, 2011, **196** 8160-8165.
- C. Cheng, Y. Wen, X. Xu, H. Gu, *J. Mater. Chem.* 2009, **19**, 8782-8788.
- Y. G. Wang and Y. Y. Xia, *J. Electrochem. Soc.*, 2006, **153**, A450-A454.

